batteries

MDPI

Article

Identifying Anode and Cathode Contributions in Li-Ion Full-Cell Impedance Spectra

Marco Heinrich [1,2,3], Nicolas Wolff [2,3], Steffen Seitz [1,3] and Ulrike Krewer [2,3,4,*]

[1] Physikalisch-Technische Bundesanstalt, 38116 Braunschweig, Germany; marcoheinrich@posteo.de (M.H.); steffen.seitz@ptb.de (S.S.)
[2] Institute of Energy and Process Systems Engineering, TU Braunschweig, 38106 Braunschweig, Germany; nicolaswolff1989@gmail.com
[3] Battery Lab Factory, TU Braunschweig, 38104 Braunschweig, Germany
[4] Institute for Applied Materials—Electrochemical Technologies, Karlsruhe Institute of Technology, 76131 Karlsruhe, Germany
* Correspondence: ulrike.krewer@kit.edu

Abstract: Measured impedance spectra of Li-ion battery cells are often reproduced with equivalent circuits or physical models to determine losses due to charge transfer processes at the electrodes. The identified model parameters can usually not readily or unambiguously be assigned to the anode and the cathode. A new measurement method is presented that enables the assignment of features of impedance spectra of full cells to single electrodes. To this end, temperature gradients are imprinted perpendicular to the electrode layers of a single-layered Li-ion battery cell while impedance spectra are measured. The method exploits different dependences of the charge transfer processes at the electrodes on temperature. An equivalent circuit model of RC-elements and the effect of temperature on the related electrode properties is discussed to demonstrate the feasibility of the method. A reliable assignment of the change of impedance spectra to the electrode processes is shown to be possible. The assignment can be used to identify if changes in an impedance spectrum originate from the anode or the cathode.

Keywords: electrochemical impedance spectroscopy; modelling; equivalent circuit model; process-identification; time constants; temperature distribution; measurement

Citation: Heinrich, M.; Wolff, N.; Seitz, S.; Krewer, U. Identifying Anode and Cathode Contributions in Li-Ion Full-Cell Impedance Spectra. *Batteries* **2022**, *8*, 40. https://doi.org/10.3390/batteries8050040

Academic Editor: Seung-Wan Song

Received: 1 March 2022
Accepted: 24 April 2022
Published: 27 April 2022

1. Introduction

Measured electrochemical impedance spectra are usually evaluated with physicochemical models [1,2] or, more frequently, with equivalent circuits [3,4] to analyse internal processes of Li-ion battery (Lib) cells. The simulations use physicochemical parameters, such as reaction constants, or circuit elements, including the charge transfer resistance, to reproduce the measured impedance spectra of full cells. It is very difficult to distinguish between effects of the anode and the cathode and to assign them to specific features of a spectrum. Usually half-cell measurements are used for this purpose but the results found on half cells can only be applied to full cells to some extent.

Many spectra of full cells include a distorted arc that is usually assigned to a superposition of two semicircles which represent charge transfer impedances at the anode and the cathode [1,5]. Independent of the shape of the spectra, unambiguous allocation of the semicircles to their respective electrodes requires prior knowledge, e.g., via half-cell measurements or property variation of single electrodes. Correct allocation, however, is crucial if anode and cathode parameters of equivalent circuit models have to be identified unambiguously. Numerous studies have analysed half cells [6–11], symmetrical cells [12–17] or cells including a reference electrode [18–22] in order to investigate the impedances of an individual electrode rather than the full cell impedance. These studies show that the time constants of the main charge transfer reactions at anode and cathode are most often

in the same order of magnitude, but not identical. This leads to the above-mentioned two overlapping arcs in an impedance spectrum which are somewhat separated from each other. To the best of our knowledge, no study has yet shown how to identify anode and cathode impedance contributions from full-cell spectra without using reference electrodes or modifying one electrode. Such information, however, will be extremely helpful to understand processes in the battery: changes of impedance spectra, e.g., due to a change of the State of Charge (SoC) or the State of Health (SoH), can be assigned to changes of the properties of the anode or the cathode [23]. Figure 1 shows measured impedance spectra of an anode half cell, a cathode half cell, and the corresponding full cell of a Li-ion battery cell. The spectrum is reduced by fitting and subtracting inductive and diffusive parts, so that only the charge transfer impedances of anode and cathode, represented by the arcs, are visible. The sum of the half-cell impedances equals the full cell impedance. In order to illustrate the issue, the full cell spectrum is simulated by an equivalent circuit model with two constant phase elements (CPE) each in parallel to a charge transfer resistance R, which we denote by CPE||R (solid blue line). Simulations on this simple model are able to reproduce the measured spectrum, but without half-cell measurements, it cannot be decided which of the two CPE||R elements must be assigned to the anode and which to the cathode.

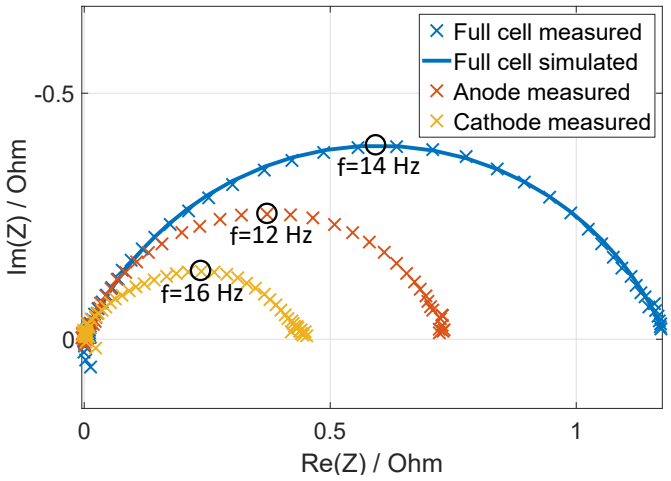

Figure 1. Nyquist plot of the impedance of cell I (60 mAh Li-ion pouch cell) with the corresponding half-cell impedances. Inductive and diffusive parts have been omitted. Measurements were conducted at room temperature and SOC 50 for the full cell.

In this study, we present a new measurement method to address this problem by using Peltier elements to imprint a temperature gradient across the width of a single-layered Li-ion cell. The basic idea to distinguish anode and cathode in the modelling of a full-cell impedance spectrum is to measure impedance spectra $Z(f)$ at different anode and cathode temperatures. Cooling down one side of the cell while heating up the other side decelerates processes in the cold electrode while processes in the warm electrode are accelerated. Both effects will be visible in the resulting full-cell impedance spectrum. A simple equivalent circuit model, consisting of two RC-elements in series has been used to analyse the corresponding full-cell impedance spectra after they have been reduced to the impedance of charge transfer processes. It will be demonstrated how to assign the semicircles of the individual charge transfer reactions to the anode and the cathode. With charge transfer reaction, we always mean the electrochemical reaction with subsequent intercalation or deintercalation. Troxler et al. [24] used a similar setup. However, they put their focus on multi-layered cells which did not allow them to heat or cool the two electrodes separately. Therefore, an assignment of electrode contributions to anode and cathode has not been done yet. We verify the robustness of our method with measurements of two batteries of the same type. The method is further supported by additional half-cell

measurements. This investigation demonstrates a method to unambiguously identify the parameters of charge transfer processes at the electrodes in impedance-based models. We will demonstrate that the new method can be used to assign parameters of simulations of full-cell spectra to the anode and the cathode. The study will demonstrate the feasibility of the method by assigning the temperature-dependent relaxation times of two RC elements to the respective temperature-dependent semi-circles of simulated impedance spectra.

2. Materials and Methods

The experimental realisation has been done with the measurement setup depicted in Figure 2. A single-layered battery cell (graphite/NiMnCo-Oxide, NMC) has been placed between two Peltier elements. In Figure 2, the anode is heated up and the cathode is cooled down. Temperatures have been measured with two PT 100 temperature sensors, which have been positioned between the Peltier elements and the anode and cathode side of the battery cell, respectively. Cooling rips and fans have been attached to the Peltier element at the cold side to increase the achievable temperature difference applied across the width of the cell. All measurements have been performed in a temperature chamber at 23 °C to ensure stable temperature. The temperature gradient across the cell is adjusted by the set temperature of the chamber and the current applied to the Peltier elements.

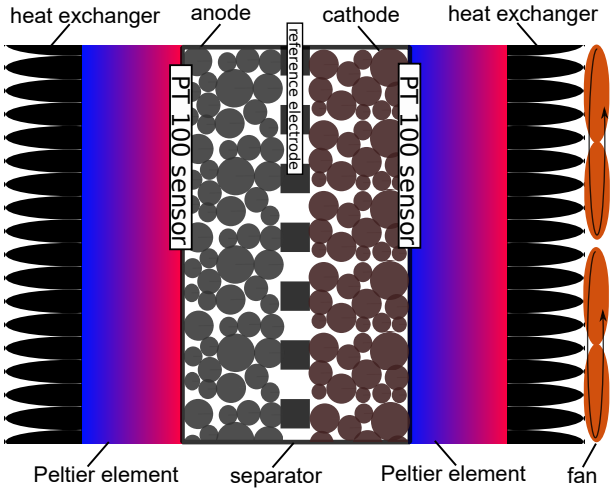

Figure 2. Schematic illustration of the measurement setup.

Two 60-mAh high-energy density Lib cells produced by Custom Cells, denoted as cell I and cell II, with roughly 17 cm² NMC and graphite electrodes respectively have been analysed with a Gamry Reference 3000 potentiostat. Both cells had a Lithium titanate (LTO) reference electrode integrated for the half-cell measurements. Measurements for the full cell were conducted as well on the cells with reference electrode. All measurements have been performed at 50% SoC referred to the nominal capacity. Impedance spectra have been measured from 0.1 Hz–10^5 Hz with an amplitude of 6 mA. The cells have been stored at room temperature and 50% SoC between the measurements.

In a first measurement, the cathode was heated up while the anode was cooled down. An impedance spectrum has been measured after the measured temperatures had stabilised. This measurement is called *Meas* 1. It took about 2 min to stabilise the temperature measured by the Peltier elements. For the results shown, we have waited 30 min to ensure a steady temperature profile across the cell. Afterwards, the warm and cold sides have been switched by turning the cell by 180° and a second impedance spectrum has been measured, called *Meas* 2.

The actual temperature profile across the cell could not be measured but has been approximated from the temperature measurements at the battery surfaces. The Peltier elements were supplied with 6.6 A and 12 V, resulting in 74 °C at the hot side and 39 °C at the cold side.

2.1. Temperature Distribution

Using the temperatures at the battery surface boundary conditions, the temperature profile within the cell can roughly be estimated. The results depend on the thermal conductivities and the thicknesses of the pouch cell bag and of the electrolyte-soaked electrodes and the separator. Thermal conductivities for similar cell materials have been used from the literature. Based on the parameters presented in Table 1, the temperature distribution shown in Figure 3 has been calculated to roughly estimate the temperature distribution. Even though the temperature difference between anode and cathode is lower compared to the measured temperatures at the Peltier elements, it is still sufficient for our purpose because the impedance of a Li-ion cell is very sensitive to changes in temperature.

Table 1. Thermal conductivities and layer thicknesses within the LiB.

Material	**Conductivity** $\mathbf{Wm^{-1}\,K^{-1}}$	**Thickness** **µm**
Pouch bag foil	0.25 [25]	125 [26]
Graphite	0.71 [27]	43.66 [28]
NMC	0.7 [27]	56.75 [28]
Separator	0.25 [25]	20 [28]

Figure 3 shows that the estimated temperature of the anode (59 °C) is 5 °C higher than the temperature of the cathode (54 °C). The thermal conductivities of anode and cathode are similar, and therefore, the temperatures of the anode and cathode will approximately be switched after the pouch cell is turned between the Peltier elements.

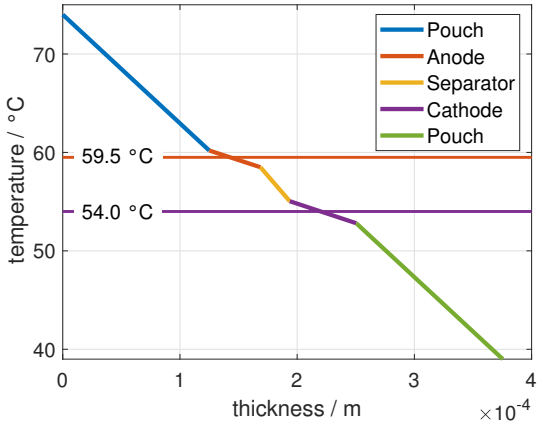

Figure 3. Estimated steady state temperature profile across the width of a single-layered Li-ion cell assuming a warm side of 74 °C and a cold side of 39 °C.

2.2. Data Evaluation Method

The procedure starts with measurement of Z_{Meas1} and Z_{Meas2} (Step1). This is followed by a modelling step (Step 2) and a model reduction step (Step 3), before the assignment of electrodes is done (Step 4). The impedance measurement results from *Meas* 1 and *Meas* 2, i.e., Z_{Meas1} and Z_{Meas2}, cannot be evaluated directly. In the upcoming sections, necessary simplifications and all steps of the data evaluation are discussed. The data evaluation strategy is displayed schematically in Figure 4.

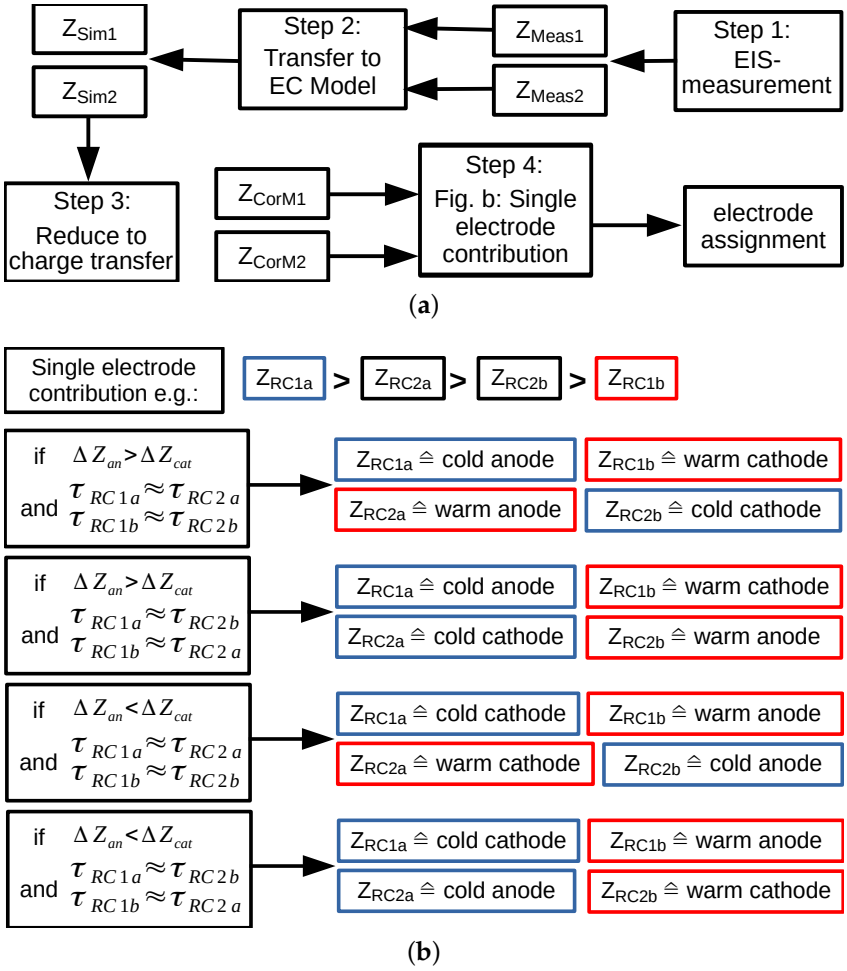

Figure 4. Schematic visualisation of the procedure to assign electrodes: (**a**) Flow diagram from first measurement to electrode assignment. (**b**) Block diagram: Four possible results for the differences of the impedances and the time constants (**left**) and the resulting electrode assignments (**right**).

2.2.1. Simplifications

In order to be able to evaluate the experimental data, assumptions about the underlying physical processes have to be made to simplify the analysis. We assume that charge transfer at the anode and cathode depends differently on temperature. As a consequence, we expect that the change of the impedance at the anode and the change of the impedance at the cathode are likewise different if the temperatures of both electrodes are switched. Therefore, we calculated the differences of the impedance spectra of the full cells *Meas* 1 and *Meas* 2 in terms of the moduli $|Z(f)|$ and the phases $\varphi(f)$ at each frequency f:

$$\Delta|Z|(f) = |Z_{Meas1}|(f) - |Z_{Meas2}|(f) \tag{1}$$

and

$$\Delta\varphi(f) = \varphi_{Meas1}(f) - \varphi_{Meas2}(f) \tag{2}$$

Note that henceforth we omit writing the frequency dependence of the impedances throughout this paper to improve readability. Following the definition of *Meas* 1 and *Meas* 2, the differences represent the effect of a warm cathode that is cooled down, superimposed by a cold anode that is heated up.

$$\Delta|Z| = (|Z_{\text{cold anode}} + Z_{\text{warm cathode}}|) - (|Z_{\text{warm anode}} + Z_{\text{cold cathode}}|) \tag{3}$$

$$\Delta\varphi = arctan\left(\frac{(Im(Z)_{\text{cold anode}} + Im(Z)_{\text{warm cathode}})}{(Re(Z)_{\text{cold anode}} + Re(Z)_{\text{warm cathode}})}\right) - arctan\left(\frac{(Im(Z)_{\text{warm anode}} + Im(Z)_{\text{cold cathode}})}{(Re(Z)_{\text{warm anode}} + Re(Z)_{\text{cold cathode}})}\right) \quad (4)$$

Data evaluation is focused on the arc of the impedance spectrum that represents charge transfer across the electrolyte/electrode interfaces at the anode and the cathode. The shape of the measured arc is affected by several physicochemical processes and properties of the cell. Basically, it is formed by the charge transfer resistances and the double layer capacitances, which would result in two superimposed semi-circles. However, solid state diffusion affects the low-frequency part of the semi-circle and inductive and capacitive effects, induced by the wires or stray capacitances, can affect the high-frequency part of the semicircle. Additionally, geometrical and material inhomogeneities lead to a distribution of time constants of the RC elements which flattens the arc [29], and the solid electrolyte interface at the electrode surface may further distort the arc. As a consequence, a comprehensive equivalent circuit to model the processes at the electrode is rather complex. A typical equivalent circuit is shown in Figure 5a and the original spectra are given in Figure 5b. For the purpose of this investigation, we have to simplify the analysis of the spectra.

Reduction of measured spectra to charge transfer processes: Here, we start by modelling the spectra Z_{Meas1} and Z_{Meas2} with the equivalent circuit given in Figure 5a to obtain Z_{Sim1} and Z_{Sim2} (step 2). After simulation, we reduce Z_{Sim} to extract the impedances of the charge transfer processes at the electrodes Z_{corM1} and Z_{corM2}. For this, we subtract impedance contributions caused by the internal resistance, diffusion, and induction. Hereby, the frequency range is unchanged. These contributions were calculated with a parameter identification algorithm in Matlab which minimises the difference between the measured absolute impedances and the sum of the assumed impedance contributions. The charge transfer impedances are represented by a resistor in parallel to a constant phase element for this purpose [4]. The equivalent circuit for this extraction process is illustrated in Figure 5a. We are aware of the fact that the surface layer on the electrodes contributes to the cell impedance as well [30]. However, the procedure works in both cases, with and without surface layer effects in impedance spectra. Figure 5b shows the measurement results for *Meas* 1 and *Meas* 2 and the same results after subtracting the impedance contributions of the internal resistance, diffusion, and induction (Z_{CorM1} and Z_{CorM2}). The respective steps are depicted in the flow diagram in Figure 4a.

We have further simplified the investigation hereafter by replacing the CPE, used to perform the reduction of the spectra, with two RC elements representing the two electrodes. Each of them consists of a charge transfer resistance R in parallel to a capacitance C. The latter is usually attributed to the double layer at the electrolyte/electrode interface. This simplification is done as the effect of a temperature change on the charge transfer processes at the electrodes can be understood more easily in terms of the charge transfer resistance and double layer capacitance compared to the rather abstract coefficients of CPE elements which cannot easily be assigned to physical quantities. Note that as the equivalent circuit used to extract the electrode impedance (Figure 5a) is only an approximation of the actual impedances of the processes in the cell, the reduced spectra that are supposed to reflect just the electrode impedances, are subject to uncertainty. Likewise, the subsequent use of the simple RC elements introduces further uncertainty. These uncertainties are acceptable as the investigation only aims to identify the arcs of an impedance spectrum with respect to the anode and the cathode rather than providing an exact model of the cell impedances. We consider the reduced spectra and the simple RC model sufficient for the proof of concept in this manuscript, in particular, because we have substantiated the results by further validation steps in Section 3.1.

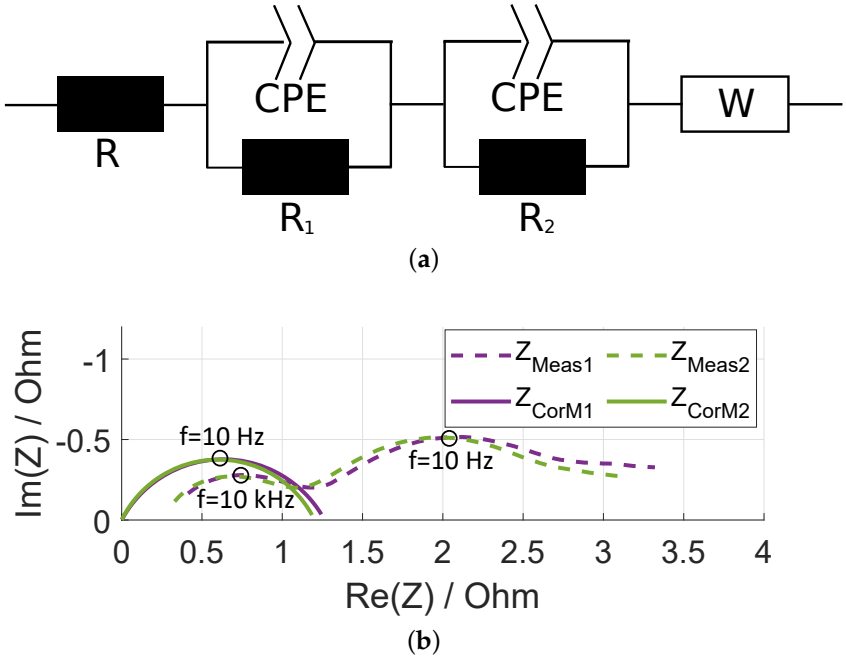

Figure 5. Reduction of electrochemical impedance spectra to charge transfer processes: (**a**) Equivalent circuit model used to reduce the measured impedance to the charge transfer processes. (**b**) Impedance of measurements 1 and 2 (dashed) and the corresponding reduced spectra after subtracting internal resistance, inductance, and diffusion (solid).

2.2.2. Assumptions for Temperature Influence

In the following, we discuss the expected effects of a temperature change on electrodes that are modelled by RC elements.

Nonlinear temperature effects: Firstly, charge transfer reactions at an electrode and diffusion in the vicinity of the electrode/electrolyte interface accelerate with increasing temperature which decreases the charge transfer resistance of the electrode. We have measured the resistances of the charge transfer reactions of the electrodes of two cells with half-cell measurements at various temperatures and found a nonlinear temperature dependence for the anode and the cathode. The results for temperatures between 5 °C and 26 °C are depicted in Figure 6. It can be seen that the change in resistance due to a change in temperature is higher for high resistances than for low resistances. It has to be noted that the resistance of the two cells differs. We attribute this to the fact that they have been made exclusively for the purpose of this investigation. Cells produced in smaller numbers usually have higher cell-to-cell variations. Since the two cells are analysed independently of each other, the difference can be accepted for this study. The assignment of the electrode impedance contributions will be done for both cells.

Temperature dependence of parameters: Secondly, we assume that the temperature change mainly affects the charge transfer resistance rather than the double layer capacitance. The effect of temperature on the double layer capacitance is difficult to assess. The double layer forms to compensate differences in the chemical potentials of the electrode and the electrolyte at the electrode/electrolyte interface. These potentials also depend on temperature. However, the relative dependence of their difference on temperature is assumed significantly smaller than that of the charge transfer resistance. This assumption is supported by the findings of Ahmed and Bade Shresthra [31]. We did comparable calculations as Ahmed and Bade Shresthra for the half-cell data of the cells used within this research and found a change of the double layer capacitance of only ≈5% for each electrode after changing the temperature from 5 °C to 17 °C.

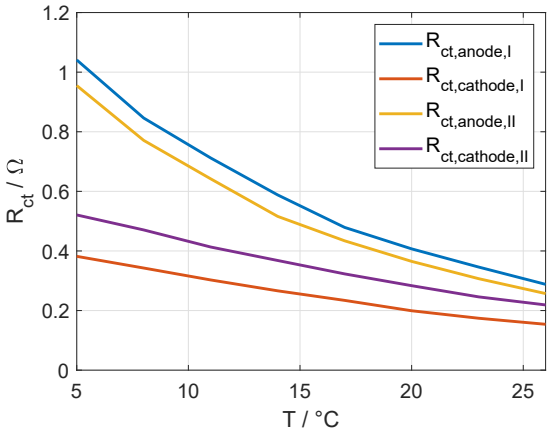

Figure 6. Charge transfer resistances of all electrodes determined with half-cell measurements of cell I and II at various temperatures.

Temperature impact on time constants: Finally, we assume that the time constant related to the charge transfer process at the electrolyte/anode interface and that related to the electrolyte/cathode interface are different but they are in the same order of magnitude. In other words, the relevant frequency ranges of the involved impedances which form the arc overlap significantly, but they are shifted against each other to some extent. This is a common property of full-cell impedance spectra which has been shown with half-cell measurements [8].

2.2.3. Identification of the Electrodes in Full-Cell Spectra

Based on the assumptions and the approach introduced in the previous sections, we now describe the general procedure of how to identify the cathode and the anode in Z_{Meas1} and Z_{Meas2}, respectively. The measurements with the different temperature configurations Z_{Meas1} and Z_{Meas2} each include the impedance contributions of both, the anode and the cathode. As seen in Equation (1), this leads to a total of four impedances affecting $\Delta|Z|$ and $\Delta\varphi$. This is exemplary shown in Figure 7 for cell I. Z_{Meas1} is modelled with two RC-elements Z_{RC1a} and Z_{RC1b} in series, representing the two electrodes. Likewise, *Meas* 2 is modelled with Z_{RC2a} and Z_{RC2b}. A nonlinear least square fitting procedure as proposed in [28] has been applied to minimise the difference between Z_{Meas1} and the sum of Z_{RC1a} and Z_{RC1b} as well as the difference between Z_{Meas2} and the sum of Z_{RC2a} and Z_{RC2b}. Please note that only the full-cell experiments were used, not the half-cell measurements. The simple model reproduces the experiments with sufficient accuracy for the analysis. Up to this point, Z_{RC1a}, Z_{RC1b}, Z_{RC2a}, and Z_{RC2b} cannot readily be assigned to the anode and cathode. This could easily be accomplished directly if the frequency ranges of the impedances contributing to the arcs do not overlap significantly. In this case, the investigation could be limited to one of the two frequency ranges. The RC-element with the impedance decreasing from *Meas* 1 to *Meas* 2 would be assigned to the anode and vice versa, because the anode has been heated up and the cathode been cooled down. However, usually, the frequency ranges overlap significantly and the identification is more complex so that it cannot be decided unambiguously how the semi-circles have changed. Therefore, further steps must be considered in order to assign Z_{RC1a}, Z_{RC1b}, Z_{RC2a}, and Z_{RC2b} to the electrodes and their corresponding temperature conditions.

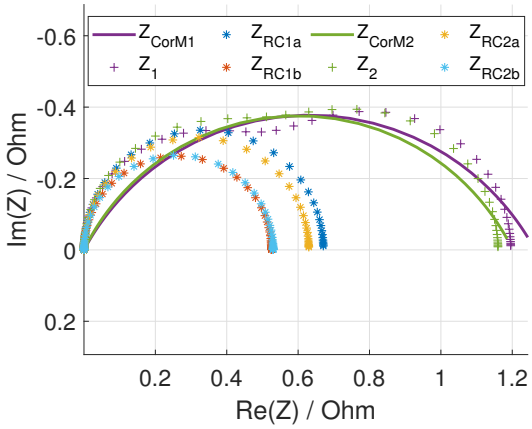

Figure 7. Reproduction of the reduced spectra from cell I: Z_{RC1a}, Z_{RC1b} represent the impedances of the RC elements of two electrodes of the first measurement, Z_1 their sum and Z_{CorM1} the corresponding (reduced) measured impedances. The impedances of the second measurement are denoted accordingly.

At low frequencies, the impedances of all four RC elements are dominated by the real part of the complex impedance. Hence, the behaviour of the real part of the impedances in this frequency range can aid in the identification process. The largest resistance must be assigned to a cold electrode, since its value must become smaller after heating up the electrode. Hence, if the largest resistance of Z_{RC1a}, Z_{RC1b}, Z_{RC2a}, and Z_{RC2b} corresponds to measurement 1, where the cathode is heated, the cold anode must be assigned to the respective impedance. This is Z_{RC1a} in the example illustrated in Figure 7. Consequently, Z_{RC1b} must obviously be assigned to the warm cathode. In turn, if the largest resistance corresponds to measurement 2, the cold cathode will be assigned accordingly. Next, the two remaining RC elements (Z_{RC2a} and Z_{RC2b} in our example) will be assigned which, at this point, cannot be uniquely attributed to cathode or anode since both fulfil the criterion that they are smaller than Z_{RC1a} and larger than Z_{RC1b}. To this end, the relaxation times $\tau = RC$ corresponding to each of the four impedances will be calculated from the resistances (R_{RC1a}, R_{RC1b}, R_{RC2a}, R_{RC2b}) and capacitances (C_{RC1a}, C_{RC1b}, C_{RC2a}, C_{RC2b}) that have been obtained from the fit. Since we assume that the double layer capacitance does not change significantly with temperature, we assign those impedances to the same electrode which has a similar capacitance. In our example, the values shown in Table 2 have been obtained. Thus, Z_{RC1a} and Z_{RC2a} are assigned to the anode and Z_{RC1b} and Z_{RC2b} are assigned to the cathode. The described procedure is schematically shown in the block diagram in Figure 4b.

Table 2. Identified resistances and capacitances with the resulting time constants for cell I.

	Resistance Ω	**Capacitance F**	**Time Constant s**	**Assignment**
Z_{RC1a}	0.671	0.0311	$2.09 \cdot 10^{-2}$	cold anode
Z_{RC1b}	0.525	0.00466	$2.44 \cdot 10^{-3}$	warm cathode
Z_{RC2a}	0.630	0.0319	$2.00 \cdot 10^{-2}$	warm anode
Z_{RC2b}	0.530	0.00464	$2.46 \cdot 10^{-3}$	cold cathode

2.2.4. Consistency Checks

Because of the uncertainties of the procedure that have been mentioned above, it is reasonable to conduct a few consistency checks to substantiate the results. First of all, it should be checked if the assigned impedance values comply with the expected temperature

behaviour that we have described above. For frequencies $f \approx 0.1$ Hz, Equation (3) can be approximated and rearranged such that

$$\begin{aligned} \Delta|Z| &= (|Z_{\text{cold anode}} + Z_{\text{warm cathode}}|) - (|Z_{\text{warm anode}} + Z_{\text{cold cathode}}|) \\ &\approx (R_{\text{cold anode}} + R_{\text{warm cathode}}) - (R_{\text{warm anode}} + R_{\text{cold cathode}}) \\ &= (R_{\text{cold anode}} - R_{\text{warm anode}}) + (R_{\text{warm cathode}} - R_{\text{cold cathode}}) \end{aligned} \quad (5)$$

The first term on the right-hand side of Equation (5) expresses the change of the resistance at the anode and the second term that of the cathode. Consequently, the sign of $\Delta|Z|$ is positive if the change of the resistance of the anode is greater than the change of the resistance of the cathode and vice versa. Thus, the RC element showing the larger change of the resistance must be assigned to the anode if $\Delta|Z|$ is positive. If $\Delta|Z|$ is negative, it must be assigned to the cathode. Additionally, the cold electrode showing the larger resistance must show the larger change because of the nonlinear temperature dependency described above. Looking at Table 2, it can easily be checked that the assignments that we have made in our example comply with these requirements. $\Delta|Z|$ is positive at the low frequency end (calculated from Equation (3)); hence, $R_{RC1a} - R_{RC1b}$ must be larger than $R_{RC2a} - R_{RC2b}$. This is schematically shown in Figure 4b.

Finally, it should be verified if the measured frequency behaviours of $\Delta|Z|$ and $\Delta\varphi$ are consistent with the modelled frequency behaviour of the impedances of the RC elements and their assignments to the electrodes. This should further substantiate the results since the investigations have been based on the Nyquist plots so far, which give, besides the relaxations times, no direct information on the frequency behaviour of the involved impedances. To this end, $\Delta|Z|$ and $\Delta\varphi$ will first be calculated from Z_{RC1a}, Z_{RC1b}, Z_{RC2a}, and Z_{RC2b}, and the assignments of these impedances to the warm and cold electrodes are performed, using Equation (3). The main features are depicted in Figure 8, which shows the moduli of Z_1, Z_2, and $\Delta|Z|$ on the left-hand side and their phases and $\Delta\varphi$ on the right-hand side. The features of the individual RC elements (not shown) are well known. The moduli of the impedances start from the associated resistance values at low frequencies and level off to zero at the high-frequency end, while the corresponding phases change from zero to $\pi/2$. The moduli and the phases of Z_1 and Z_2 show a similar behaviour. However, $\Delta|Z|$ and $\Delta\varphi$ can show quite different features, depending on the values of the involved resistances and capacitances. Figure 8 shows the features under the conditions that we have assumed, i.e.,

- The resistance values are in the same order of magnitude;
- The largest resistance is assigned to a cold anode;
- The change of the resistance at the anode and the cathode is smaller than the difference of the anode and cathode resistance;
- The double layer capacitance of the anode and the cathode are in the same order of magnitude;
- The double layer capacitance at an electrode does not change significantly with temperature.

The main features that can be observed are:

- $\Delta|Z|$ first decreases with increasing frequency. It is positive at the low-frequency end because RC1a has been assigned to the cold anode, i.e., the highest resistance. With increasing frequency, the moduli of Z_1 and Z_2 cross each other. As a consequence, their difference becomes negative, and then, it shows a minimum. At high frequencies, $\Delta|Z|$ gradually levels off to zero. If the highest resistance is assigned to the cold cathode, $\Delta|Z|$ will be negative at the low frequencies and it will show a maximum.
- $\Delta\varphi$ approaches zero at the low- and high-frequency end. It has a minimum at lower frequencies and a maximum at larger frequencies.

At the high-frequency end, one could expect that ΔZ and $\Delta\varphi$ are dominated by the processes showing the smallest relaxation times, i.e., the warm electrodes since the slower processes do contribute less to the total impedance in this region. However, we have found that the significant overlap of the frequency ranges of the four impedances involved,

including eight parameters, make it difficult to assign specific features seen in the high-frequency range to the warm electrodes. In the next section, we apply the described data evaluation procedure to our measured data.

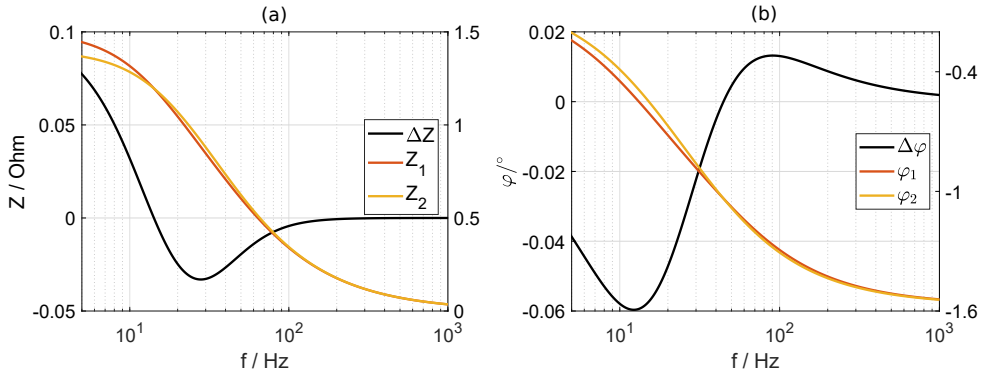

Figure 8. Simulation results of the introduced *RC*-element model. (**a**) Z_1 and Z_2 each represent the total impedance of two *RC*-elements and $\Delta|Z| = |Z_1| - |Z_2|$. The corresponding phases are depicted in (**b**).

3. Results

3.1. Method Application to Experimental Data

We have performed the procedure described in Sections 2 and 2.2 with two cells of the same type in order to verify the reproducibility. The spectra already shown in Figures 5b and 7 depict the results of cell I. The spectra of cell II (not shown) have a comparable behaviour. Tables 2 and 3 list the identified values of the four RC impedances Z_{RC1a}, Z_{RC1b}, Z_{RC2a}, and Z_{RC2b} for cell I and cell II, respectively. Following the reasoning of the simulations made in Section 2.2.3, Z_{RC1a} and Z_{RC2a} of the measurement have to be assigned to the anode and Z_{RC1b} and Z_{RC2b} have to be assigned to the cathode.

Table 3. Identified resistances and capacitances with the resulting time constants for cell II.

	Resistance **Ω**	**Capacitance** **F**	**Time Constant** **s**	**Assignment**
Z_{RC1a}	0.654	0.0282	$1.84 \cdot 10^{-2}$	cold anode
Z_{RC1b}	0.163	0.00534	$8.70 \cdot 10^{-4}$	warm cathode
Z_{RC2a}	0.595	0.0285	$1.70 \cdot 10^{-2}$	warm anode
Z_{RC2b}	0.172	0.00532	$9.15 \cdot 10^{-4}$	cold cathode

The absolute resistance and capacity values of the two cells differ to some extent due to manufacturing variability and possible additional errors from the simplifications described in Section 2.2.2.

Figure 9a,b shows the frequency behaviour of $\Delta|Z|$ and $\Delta\varphi$ of cell I and cell II, respectively. Qualitatively, their frequency behaviours fit well to the simulation results illustrated in Figure 8. $\Delta|Z|$ is positive at the low-frequency end, decreases with increasing frequency, changes its sign in the mid-frequency range and shows a minimum before its starts to level off. The phase difference shows a minimum and rises above zero to another maximum, which seems to be beyond the investigated frequency range for cell II. Therefore, the analysis of the frequency dependency of the measurement data supports or, at least, does not falsify the conclusion that the anodes in the measured cells have a higher charge transfer resistance and a higher time constant than the cathode. The frequency behaviour of $\Delta|Z|$ and $\Delta\varphi$ of both cells is qualitatively the same which substantiates the robustness of the procedure qualitatively.

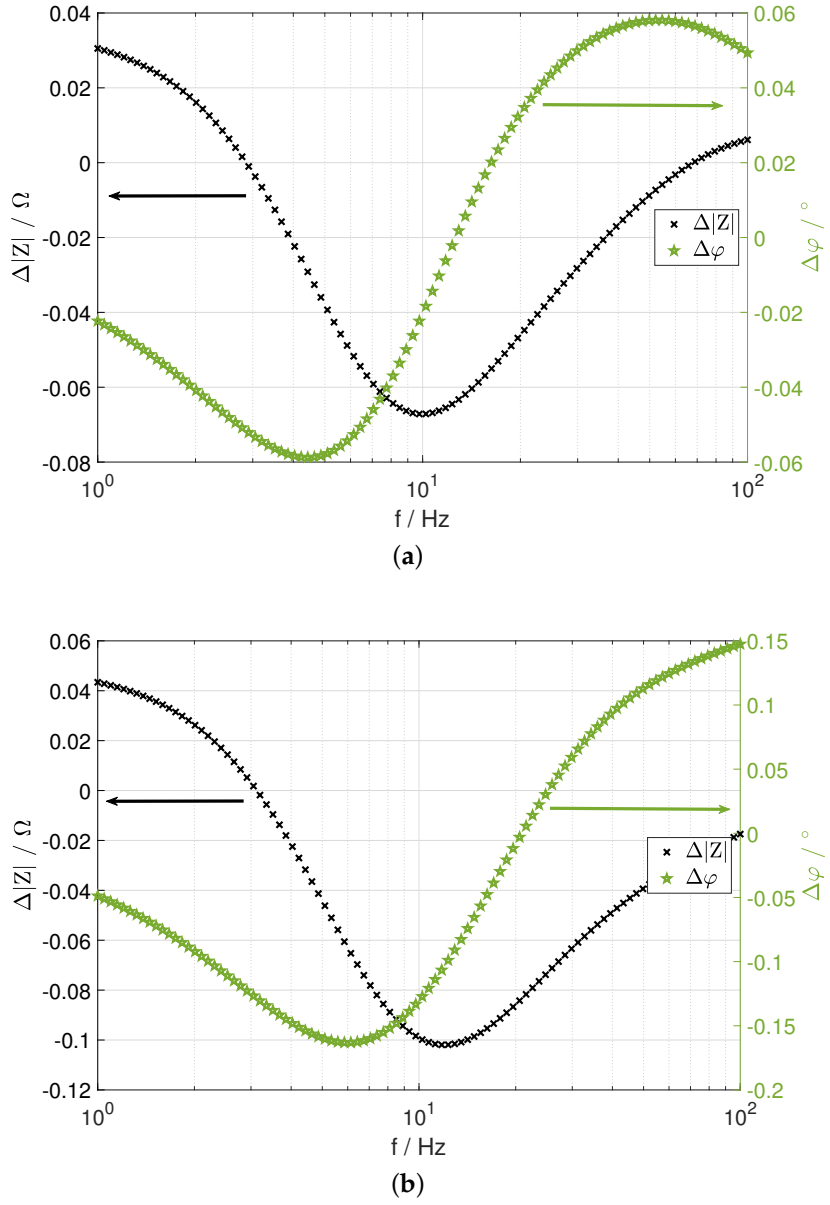

Figure 9. Differences between *Meas* 1 and *Meas* 2 for the impedance (black ✖, calculated with Equation (1)) and the phase angle (green ★, calculated with Equation (2)) with a temperature gradient from ≈54.0–59.5 °C. (**a**) Cell I. (**b**) Cell II.

3.2. Validation of the Assignments with Half-Cell Measurements

Half-cell measurements have been additionally performed to verify the attribution of electrodes and thus our methodology. To this end, the anode and cathode impedances have been simultaneously measured with the impedances of the full cell to determine the relaxation times of the related charge transfer impedance independently. It should be noted that the sum of the imaginary parts of the half-cell measurements equals those of the corresponding full-cell measurements, which also holds for the sum of the real parts. This proves that the three-electrode arrangement cell can be used to split the measured full-cell impedances into the contributions of the individual electrodes. The untreated results are shown in Figure 10a,b which depicts the imaginary parts of the impedances over the frequency. The reciprocal of the characteristic frequency at the minimum of the imaginary part corresponds to the relaxation time of the charge transfer impedance of an electrode, assuming that it is determined by the behaviour of an RC element as described

in Section 2.2.1. Table 4 lists the relaxations times of the electrodes under warm and cold conditions and compares them to those derived by our method. The relaxation times derived from the half-cell measurements confirm the assignment of relaxations times to anode and cathode from the full-cell measurements. The differences in absolute values may be attributed to our simplifications as mentioned above. Nevertheless, the half-cell measurements support the simulated results, in particular, the result that the anode has a higher charge transfer resistance and a higher relaxation time.

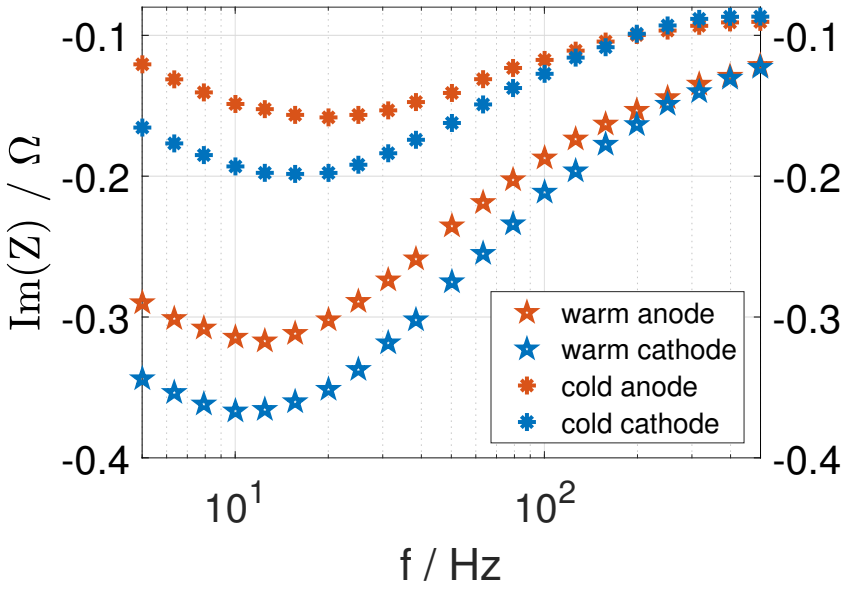

(**a**)

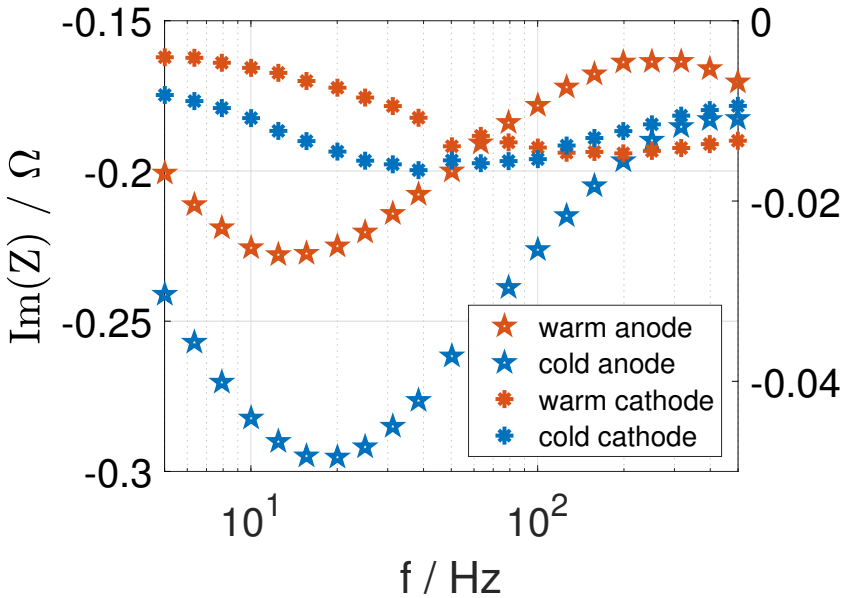

(**b**)

Figure 10. Imaginary part of the impedance for half-cell measurements with a temperature distribution from ≈54–59 °C. Left axis shows anode values and right axis shows cathode values. (**a**) Cell I. (**b**) Cell II.

Table 4. Comparison of measured and simulated relaxation times (all given in seconds) of both electrodes of both cells.

	Time constants of the simulation in seconds			
	cold cathode	warm anode	cold anode	warm cathode
Cell I	0.002	0.020	0.021	0.002
Cell II	0.001	0.017	0.018	0.001
	Time constants of the experiment in seconds			
	cold cathode	warm anode	cold anode	warm cathode
Cell I	0.011	0.013	0.013	0.008
Cell II	0.004	0.011	0.008	0.002

4. Conclusions

In this work, we have presented a new method which enables to assign anode and cathode impedance contributions solely with measurements on full-cell LiBs. A temperature gradient is applied on a single-layered Li-ion battery cell and exploits different dependences of the anode and cathode charge transfer processes on temperature. Feasibility has been demonstrated by reproducing the measurement results with a simple model of RC elements showing that the method is suitable to decide if the identified parameters of an electrode process used for the simulation should be assigned to the anode or the cathode. The assignment has been substantiated by further consistency tests and been proven with half-cell measurements. Knowledge about the anode and cathode contributions to the overall full-cell behaviour improves the possibility to evaluate various kinds of characterisation measurements. Impact of changes of the measurement conditions, i.e., temperature, SoC or SoH can be assigned to a specific electrode more easily if the introduced method is applied in advance. The method might be optimised by increasing the temperature gradient across the cell, by decreasing the effects disturbing the electrode impedances, or by measuring the impedances at various temperatures. Future studies which comprise electrode manufacturers may also target to proof all cases shown in Figure 4, while this study is just be a proof of the principle. However, once the impedance contribution of a specific process is assigned to its related electrode, this information can be used for more sophisticated models to simulate the impedance spectra of other cells of the same cell chemistry, cell balancing, and electrode particle sizes. The introduced method might not be limited to Lithium-ion cells but could also be suitable for, e.g., Li-S cells [32,33].

Author Contributions: Conceptualization, M.H. and U.K.; methodology, M.H. and N.W.; software, M.H.; validation, M.H. and S.S.; writing—original draft preparation, M.H.; writing—review and editing, S.S.; supervision, U.K. All authors have read and agreed to the published version of the manuscript.

Funding: This research received no external funding.

Institutional Review Board Statement: Not applicable.

Informed Consent Statement: Not applicable.

Data Availability Statement: Not applicable.

Conflicts of Interest: The authors declare no conflicts of interest.

References

1. Doyle, M.; Meyers, J.P.; Newman, J. Computer Simulations of the Impedance Response of Lithium Rechargeable Batteries. *J. Electrochem. Soc.* **2000**, *147*, 99. [CrossRef]
2. Xie, Y.; Li, J.; Yuan, C. Mathematical Modeling of the Electrochemical Impedance Spectroscopy in Lithium Ion Battery Cycling. *Electrochim. Acta* **2014**, *127*, 266–275. [CrossRef]
3. Levi, M.D.; Aurbach, D. Simultaneous Measurements and Modeling of the Electrochemical Impedance and the Cyclic Voltammetric Characteristics of Graphite Electrodes Doped with Lithium. *J. Phys. Chem. B* **1997**, *101*, 4630–4640. [CrossRef]
4. Huang, R.W.J.M.; Chung, F.; Kelder, E.M. Impedance Simulation of a Li-Ion Battery with Porous Electrodes and Spherical Li+ Intercalation Particles. *J. Electrochem. Soc.* **2006**, *153*, A1459. [CrossRef]
5. Sikha, G.; White, R.E. Analytical Expression for the Impedance Response for a Lithium-Ion Cell. *J. Electrochem. Soc.* **2008**, *155*, A893–A902. [CrossRef]
6. Abraham, D.P.; Knuth, J.L.; Dees, D.W.; Bloom, I.; Christophersen, J.P. Performance degradation of high-power lithium-ion cells-Electrochemistry of harvested electrodes. *J. Power Source* **2007**, *170*, 465–475. [CrossRef]
7. Shafiei Sabet, P.; Sauer, D.U. Separation of predominant processes in electrochemical impedance spectra of lithium-ion batteries with nickel–manganese–cobalt cathodes. *J. Power Source* **2019**, *425*, 121–129. [CrossRef]
8. Shafiei Sabet, P.; Stahl, G.; Sauer, D.U. Non-invasive investigation of predominant processes in the impedance spectra of high energy lithium-ion batteries with Nickel-Cobalt-Aluminum cathodes. *J. Power Source* **2018**, *406*, 185–193. [CrossRef]
9. Schindler, S.; Danzer, M.A. Influence of cell design on impedance characteristics of cylindrical lithium-ion cells: A model-based assessment from electrode to cell level. *J. Energy Storage* **2017**, *12*, 157–166. [CrossRef]
10. Mussa, A.S.; Liivat, A.; Marzano, F.; Klett, M.; Philippe, B.; Tengstedt, C.; Lindbergh, G.; Edström, K.; Lindström, R.W.; Svens, P. Fast-charging effects on ageing for energy-optimized automotive LiNi 1/3 Mn 1/3 Co 1/3 O 2 /graphite prismatic lithium-ion cells. *J. Power Source* **2019**, *422*, 175–184. [CrossRef]
11. Guo, M.; Meng, W.; Zhang, X.; Liu, X.; Bai, Z.; Chen, S.; Wang, Z.; Yang, F. Electrochemical behavior and self-organization of porous Sn nanocrystals@acetylene black microspheres in lithium-ion half cells. *Appl. Surf. Sci.* **2019**, *470*, 36–43. [CrossRef]
12. Illig, J.; Chrobak, T.; Ender, M.; Schmidt, J.; Klotz, D.; Ivers-Tiffée, E. Studies on LiFePO 4 as cathode material in Li-ion batteries. *ECS Trans.* **2010**, *28*, 3–17. [CrossRef]
13. Tong, B.; Wang, J.; Liu, Z.; Ma, L.; Zhou, Z.; Peng, Z. Identifying compatibility of lithium salts with LiFePO4 cathode using a symmetric cell. *J. Power Source* **2018**, *384*, 80–85. [CrossRef]
14. Kisu, K.; Aoyagi, S.; Nagatomo, H.; Iwama, E.; Reid, M.T.H.; Naoi, W.; Naoi, K. Internal resistance mapping preparation to optimize electrode thickness and density using symmetric cell for high-performance lithium-ion batteries and capacitors. *J. Power Source* **2018**, *396*, 207–212. [CrossRef]
15. Conder, J.; Villevieille, C.; Trabesinger, S.; Novák, P.; Gubler, L.; Bouchet, R. Electrochemical impedance spectroscopy of a Li–S battery: Part 1. Influence of the electrode and electrolyte compositions on the impedance of symmetric cells. *Electrochim. Acta* **2017**, *244*, 61–68. [CrossRef]
16. Petibon, R.; Sinha, N.N.; Burns, J.C.; Aiken, C.P.; Ye, H.; Vanelzen, C.M.; Jain, G.; Trussler, S.; Dahn, J.R. Comparative study of electrolyte additives using electrochemical impedance spectroscopy on symmetric cells. *J. Power Source* **2014**, *251*, 187–194. [CrossRef]
17. Chen, C.H.; Liu, J.; Amine, K. Symmetric cell approach and impedance spectroscopy of high power lithium-ion batteries. *J. Power Source* **2001**, *96*, 321–328. [CrossRef]
18. Abraham, D.P.; Poppen, S.D.; Jansen, A.N.; Liu, J.; Dees, D.W. Application of a lithium-tin reference electrode to determine electrode contributions to impedance rise in high-power lithium-ion cells. *Electrochim. Acta* **2004**, *49*, 4763–4775. [CrossRef]
19. Nara, H.; Mukoyama, D.; Yokoshima, T.; Momma, T.; Osaka, T. Impedance Analysis with Transmission Line Model for Reaction Distribution in a Pouch Type Lithium-Ion Battery by Using Micro Reference Electrode. *J. Electrochem. Soc.* **2016**, *163*, A434–A441. [CrossRef]
20. Gómez-Cámer, J.L.; Novák, P. Electrochemical impedance spectroscopy: Understanding the role of the reference electrode. *Electrochem. Commun.* **2013**, *34*, 208–210. [CrossRef]
21. Dondelinger, M.; Swanson, J.; Nasymov, G.; Jahnke, C.; Qiao, Q.; Wu, J.; Widener, C.; Numan-Al-Mobin, A.M.; Smirnova, A. Electrochemical stability of lithium halide electrolyte with antiperovskite crystal structure. *Electrochim. Acta* **2019**, *306*, 498–505. [CrossRef]
22. Raijmakers, L.H.; Lammers, M.J.; Notten, P.H. A new method to compensate impedance artefacts for Li-ion batteries with integrated micro-reference electrodes. *Electrochim. Acta* **2018**, *259*, 517–533. [CrossRef]
23. Heinrich, M. Electrochemical Impedance Spectroscopy on ageing Lithium-Ion Batteries. Ph.D. Thesis, Technische Universität Braunschweig, Braunschweig, Germany, 2020.
24. Troxler, Y.; Wu, B.; Marinescu, M.; Yufit, V.; Patel, Y.; Marquis, A.J.; Brandon, N.P.; Offer, G.J. The effect of thermal gradients on the performance of lithium-ion batteries. *J. Power Source* **2014**, *247*, 1018–1025. [CrossRef]
25. Burheim, O.S.; Onsrud, M.A.; Pharoah, J.G.; Vullum-Bruer, F.; Vie, P.J.S. Thermal Conductivity, Heat Sources and Temperature Profiles of Li-Ion Batteries. *ECS Trans.* **2014**, *58*, 145–171. [CrossRef]
26. Korthauer, R. *Handbuch Lithium-Ionen-Batterien*; Springer: Berlin/Heidelberg, Germany, 2013.

27. Richter, F.; Vie, P.J.; Kjelstrup, S.; Burheim, O.S. Measurements of ageing and thermal conductivity in a secondary NMC-hard carbon Li-ion battery and the impact on internal temperature profiles. *Electrochim. Acta* **2017**, *250*, 228–237. [CrossRef]
28. Heinrich, M.; Wolff, N.; Harting, N.; Laue, V.; Röder, F.; Seitz, S.; Krewer, U. Physico-Chemical Modeling of a Lithium-Ion Battery: An Ageing Study with Electrochemical Impedance Spectroscopy. *Batter. Supercaps* **2019**, *2*, 530–540. [CrossRef]
29. Kaplan, T.; Gray, L.J.; Liu, S.H. Self-affine fractal model for a metal-electrolyte interface. *Phys. Rev. B* **1987**, *35*, 5–7. [CrossRef]
30. Gaddam, R.R.; Katzenmeier, L.; Lamprecht, X.; Bandarenka, A.S. Review on physical impedance models in modern battery research. *Phys. Chem. Chem. Phys.* **2021**, *23*, 12926–12944. [CrossRef]
31. Ahmed, S.H.; Bade Shrestha, S.O. Temperature Dependence of Double Layer Capacitance in Lithium-Ion Battery. In Proceedings of the 116th IIER International Conference, Phuket, Thailand, 9–10 August 2017; pp. 7–10.
32. Xing, Z.; Tan, G.; Yuan, Y.; Wang, B.; Ma, L.; Xie, J.; Li, Z.; Wu, T.; Ren, Y.; Shahbazian-Yassar, R.; et al. Consolidating Lithiothermic-Ready Transition Metals for Li2S-Based Cathodes. *Adv. Mater.* **2020**, *32*, 2002403. [CrossRef]
33. Tan, G.; Xu, R.; Xing, Z.; Yuan, Y.; Lu, J.; Wen, J.; Liu, C.; Ma, L.; Zhan, C.; Liu, Q.; et al. Burning lithium in CS2 for high-performing compact Li2S–graphene nanocapsules for Li–S batteries. *Nat. Energy* **2017**, *2*, 1–10. [CrossRef]